CloudSat Project

A NASA Earth System Science Pathfinder Mission

Level 2B Fluxes and Heating Rates with Lidar [2B-FLXHR-LIDAR] Process Description and Interface Control Document

Version: P2 R05

Date: January, 2023

Contact

Questions concerning the document and proposed changes shall be addressed to:

David Henderson   Tristan L'Ecuyer
dshenderson@wisc.edu   OR   tristan@aos.wisc.edu

Contents

1 Introduction

1.1 Overview

This document provides an overview of the 2B-FLXHR-LIDAR flux and heating rate algorithm for CloudSat. Please note the 2B-FLXHR Radar Only product is no longer supported. The objective of the algorithm is to make use of liquid and ice water content estimates from the CPR to produce estimates of broadband fluxes and heating rates for each radar profile. 2B-FLXHR-LIDAR includes measurements from CALIPSO and MODIS; additional CALIPSO and MODIS data will provide properties for clouds and aerosol undetected by CloudSat. For a particular radar profile, upwelling and downwelling longwave and shortwave flux profiles are calculated at discrete levels of the atmosphere. Corresponding heating rates are inferred from these fluxes. In order to perform these calculations, the algorithm makes use of a combination of atmospheric state variables obtained from ECMWF reanalysis data, profiles of cloud ice and liquid water content obtained from the CloudSat 2B-CWC-RO and 2C-ICE products, and surface albedos obtained from seasonally-varying maps of surface reflectance properties. LWC and IWC from undetected clouds are estimated from optical depths reported by collocated MODIS data (MOD06-1KM-AUX), CALIOP backscatter-based estimates, and CALIPSO's CAL_LID_L2_05kmCLay products. Aerosol location and optical depth are obtained from CALIPSO's CAL_LID_L2_05kmALay product. Precipitation estimates are also reported through the 2C-Precip-Coumn product from CloudSat. The remainder of this document describes the algorithm in greater detail. The algorithm will be referred as the 2B-FLXHR-LIDAR algorithm throughout documentation for simplification.

1.2 Major Changes in Release 05

The primary changes since Release 04 have concentrated on improving cloud microphysical assumptions and surface characteristics. Further, we now use CALIPSO V4 inputs and include outputs for vertically resolved cloud optical depth. New variables are now included for top-of-atmpshere fluxes. A brief descripion of the specific changes include:

- All CloudSat data ingested into the retrieval are Release Version 05.

- CALIPSO V4 Cloud and Aerosol products are used to supplement cloud detection and optical properties.

- New top-of-atmosphere flux variables are included. These fluxes use seasonal ECMWF data modeled above the CloudSat profile to provide a more accurate estimates. Variable names are: FU_TOA, FU_NC_TOA, FU_NA_TOA, and FD_TOA_IncomingSolar.

- Vertically resolved cloud optical depth is now included in output.

- Improved land and ocean surface albedos.

- Longwave land emissivity now varies by surface type.

- Cloud detection now consistent with 2B-CLDCLASS-LIDAR

- Supercooled liquid now explicitly represented when identified by 2B-CLDCLASS-LIDAR.

- Ice properties included from 2C-ICE when 2B-CWC-RO has no data.

- CloudSat MODIS auxilary product MOD06-1KM-AUX used to constrain cloud properties in single layer cloud profiles and where 2B-CWC-RO is flagged for possible precipitation.

- Various bug fixes.

More detailed descriptions of the improved land properties and use of 2C-ICE can be found in Matus et al. [18]. Description and validation of supercooled liquid can be found in Van Trict et al [20] and McIllhatten et al [19].

1.3 Change Log for Release 05 Product 2 (R05 P2)

Note Major changes for the original R05 are listed above. The Release Version R05 P2 fixes various bugs that produced data flagged as missing. Further, due to an error in ECMWF-AUX, this 2B-FLXHR-lidar release will now use the corrected ECMWF-AUX product. Please see the ECMWF-AUX documentation for details on the correction.

Specific changes include:

- An updated version of ECMWF-AUX is now used to correct issues in temperature and humidity interpolation.

- Added fill values for missing 2B-CWC-RO data due to unclassified data in 2B-CLDCLASS. When possible, data is interpolated from nearby valid cloud properties. Data is flagged in the status flag as values 06 or 07; Filled LWC or Filled IWC. Missing data might still persist in regions, such as near cloud edges, where interpolation is not possible.

- Fixed issue where LW fluxes were reported missing, but the SW fluxes were valid.

- Fixed issue where geometrically thin CALIPSO-only detected clouds resulted in missing data.

- Fixed incorrect Missing CALIPSO data status flag in columns containing aerosol.

2 Algorithm Theoretical Basis

2.1 Overview

The core of the algorithm employs a broadband, two-stream, plane-parallel doubling-adding radiative transfer model. The general structure of the algorithm is similar to that described by Ritter and Geleyn [4]. The particular parameterizations and performance of the algorithm are described by Stephens et al. [1]. The model utilizes a delta-Eddington formulation in six shortwave bands and a constant-hemisphere formulation in twelve longwave bands. An appropriate set of atmospheric state variables and retrieved cloud ice/liquid water contents are used to calculate the vertical profile of band-resolved optical properties. These optical properties are then used to describe the reflectance (R), transmission (T) and radiative source (Σ) characteristics of each slab. By combining R, T, and Σ systematically for multiple slabs using the interaction principle, the broadband radiative fluxes at each slab face can be calculated. By calculating the amount of flux absorbed or emitted by each slab, the rate of radiative heating in each slab can be determined. Finally, the broadband fluxes and heating rates are aggregated to the spectral resolution of the FLXHR product and reported with the required vertical resolution.

2.2 Radiative Transfer Model

2.2.1 Two-stream formulation

The optical properties for a single homogeneous slab can be described in terms of its bulk, or "global", bidirectional reflectance, R, global bidirectional transmission, T, and global radiative source properties, Σ. For such a slab with faces labelled "a" and "b", once R, T, and Σ are determined the solution to the two-stream monochromatic radiative transfer equation can be written as:

$$F_a^+ = RF_a^- + TF_b^+ + \Sigma^+$$

$$F_b^- = RF_b^+ + TF_a^- + \Sigma^-$$

where superscript "+" indicates a quantity directed in the "$b \to a$" direction and a superscript "−" indicates a quantity directed in the "$a \to b$" direction. Given the fluxes F_a^- and F_b^+ at the layer boundaries, the two remaining fluxes can be determined. For an n-layer atmosphere, a tridiagonal system of $2n+2$ coupled equations can be written in similar form and solved recursively using the adding relations described by Stephens and Webster [2]. Stephens et al. [1] show that the computational expense for this sort of scheme increases linearly with the number of atmospheric layers, making it attractive for use on data which is highly vertically resolved, such as that that will be produced by CloudSat.

R, T, and Σ depend on the optical depth, τ, the single scattering albedo, ω_0, (the ratio of the scattering coefficient to the extinction coefficient) and the asymmetry parameter g (the fraction of the incident energy that is scattered in the forward direction) of the matter in the layer. The particular form of R, T, and Σ depend on the nature of the radiative source and on which formulation is being used. In the solar wavelengths, the radiative source is due to scattering of the direct solar beam and the delta-Eddington method is employed. In the longwave spectrum, the radiative source is due to thermal emission of the atmosphere and the constant hemisphere method is used. Stephens et al. [1] studied a range of radiative transfer scenarios produced by a global climate model and evaluated the performance of two-stream delta-Eddington, two-stream constant hemisphere, and four-stream solution techniques. For the bulk of the solar radiative transfer scenarios, the delta-Eddington method produced superior results compared to the other two. For longwave radiative transfer, the constant hemisphere method proved superior.

To obtain τ, ω_0, and g for the layer as a whole, the optical properties of the components of the layer must be evaluated. In general, τ, ω_0, and g for each material will vary spectrally but this spectral variation over some of the narrow spectral bands, employed in the 2B-FLXHR-LIDAR algorithm is negligible. Consequently, while some optical properties must be treated as spectrally variant, others, where possible, are approximated to be grey (invariant within the spectral band) in the interest of computational efficiency. In general, layer τ, ω_0, and g can include any combination of the following processes: Rayleigh scattering, gaseous absorption, and both absorption and scattering by condensed water.

2.2.2 Method of solution

The 2B-FLXHR-LIDAR radiative transfer algorithm performs independent flux calculations over twelve longwave bands and six solar bands. These bands are summarized in Table 1. Ultimately these bands are combined into the two broadband flux estimates, one over the longwave and the other over the shortwave, that are ultimately reported by the algorithm.

Table 1: Bands used by 2B-FLXHR-LIDAR.

Longwave (LW)		Shortwave (SW)	
Band Limits, μm	corr. k Intervals	Band Limits, μm	Corr. k Intervals
4.55 - 5.26	2	0.20 - 0.69	10
5.26 - 5.88	3	0.69 - 1.23	8
5.88 - 7.14	4	1.23 - 1.90	12
7.14 - 8.00	4	1.90 - 2.50	7
8.00 - 9.09	3	2.50 - 3.51	12
9.09 - 10.20	5	3.51 - 4.00	5
10.20 - 12.50	2		
12.50 - 14.92	10		
14.92 - 18.51	12		
18.51 - 25.00	7		
25.00 - 35.71	7		
35.71 - ∞	8		

The principal steps in the execution of the 2B-FLXHR-LIDAR algorithm are summarized in Figure 1. Calculations are done for each band sequentially. For each band, the algorithm proceeds by first computing and combining the optical properties for the gases in each atmospheric layer. Then a loop over spectral intervals is performed in which the spectrally varying cloud optical properties are computed, combined with the atmospheric optical properties, then used in a two-stream calculation to compute the fluxes in the spectral interval. As the loop continues, the spectral fluxes are summed to produce the band flux, then the band heating rates are computed. The set of shortwave and longwave fluxes and heating rates are then output at the maximum vertical resolution of the CPR and the 2B-CWC product, i.e. 240 m. This output forms the 2B-FLXHR-LIDAR product.

For the solar bands, molecular (Rayleigh) scattering and condensed water optical properties are treated as grey properties. Rayleigh optical thicknesses for all layers are calculated using a parameterization based on the central wavelength of the band, the layer pressure, and the pressure thickness of the layer. Additionally, refractive effects are considered in the visible band. The optics of condensed water particles are obtained from anomalous diffraction theory (ADT) using parameterizations derived from Stephens et al. [5] and Mitchell et al. [12]. Cloud particle distributions are described using a modified gamma size distribution with effective radii of 13 μm for liquid droplets and 30 μm for ice particles.

For longwave bands, the condensed water optics are considered grey along with water vapor continuum absorption and Planck emission. Condensed water optics are parameterized using ADT as mentioned above with the exception that, for longwave bands, precalculated values of asymmetry parameters for each band are used. Absorption by the water vapor continuum is treated using a parameterization developed from the water vapor continuum of CKD 2.1 by Clough et al. [13]. The general method of implementation for the correlated-k treatment of the gaseous absorption is described by Lacis and Oinas [14]. The details of this particular implementation are described in Fu and Liou [3].
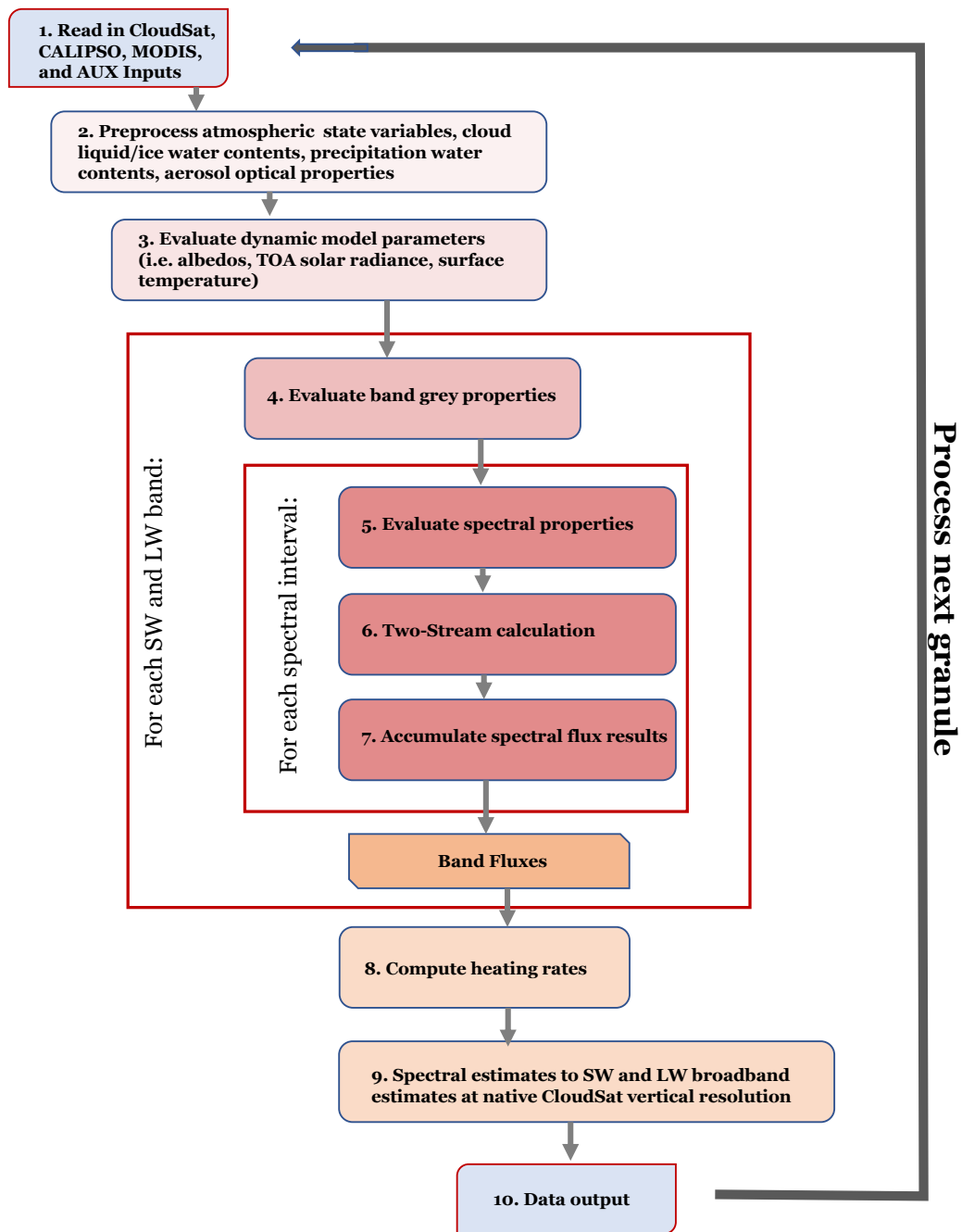
Figure 1: Flow diagram of the steps in the execution of the 2B-FLXHR-LIDAR algorithms.

2.2.3 Implementation

The CloudSat 2B-FLXHR-LIDAR retrieval generally follows the process outlined in Henderson et al [16]. The algorithm is only run when cloud-free or cloudy scenes with valid cloud mask data are available through any of the previous mentioned products and passes its internal quality control (QC) criteria. 2B-FLXHR-LIDAR will also run if aerosol is present in the CALIPSO CAL_LID_L2_05kmALay product. Some specific features of the implementation are summarized as follows:

1. The top boundary condition (top of atmosphere) consists of zero downwelling longwave flux and a nonzero downwelling solar flux adjusted for the eccentricity of the earth's orbit.

2. Shortwave calculations are optimized so that flux calculations are only done for daylit columns.

3. Evaluations of Planck emission are done using a polynomial expression to improve speed.

4. The lower boundary condition (bottom of atmosphere) for longwave calculation is an upwelling flux from the surface based on the surface temperature and an emissivity less than 1, which is defined as a function of surface type using tables from Huang et al [21]. The lower boundary condition for each shortwave calculation assumes the surface behaves as a lambertian reflector. The algorithm is implemented such that one albedo may be used for the visible bands, another used for all near-IR bands.

5. Cloud liquid and ice water are assumed to be uniformly distributed in layers where cloud is present (no fractional cloudiness).

6. 2B-FLXHR-LIDAR uses the radar-only version of the 2B-CWC, but is supplemented by optical depths from the MOD06-1KM-AUX product (when available) for a single layer of cloud in each vertical column. Cirrus cloud properties detected only by CALIOP are calculated using a lidar-transmission method mentioned later in Section 3.2.2. If cloud is detected by CALIOP, but not the CloudSat mask and no microphysical information is available climatological values are used: For liquid, water content of 0.08 gm^{-3} and effective radius of 10 um. For ice, water content of 0.0015 gm^{-3} and effective radius of 30 um.

7. Effective ice radii and water contents from 2C-ICE are used in cloud layers detected by CALIPSO products above the freezing layer where no information from 2B-CWC-RO is available.

8. Cloud water and precipitation water content are partitioned into liquid and ice according to the rain top found in 2C-PRECIP-COLUMN. Liquid water is decreased linearly from freezing level to rain top. Cases where rain top is not defined, water is decreased lineraly to 263 K temperature level.

9. In precipitation, where the 2B-CWC algorithm generally fails to converge, 2B-FLXHR-LIDAR will fill rain water contents consistent with a Marshall-Palmer distribution up to the 2C-PRECIP-COLUMN defined rain top height. If 2C-PRECIP-COLUMN data is not available the algorithm assumes a value of 0.15 gm^{-3} for rainfall or 0.02 gm^{-3} for drizzle for the water contents of all cloud filled bins up to the freezing level. Cloud water contents of 0.10 gm^{-3} are included from the LCL to rain top or 263 K temperature level as described above.

10. If 2B-CWC-RO is valid and flagged for possible precipitation the effective radius and liquid water content are scaled using the MOD06-1KM-AUX product. In multi-layered cloud cases, the effective radius and liquid water content are scaled in the lowest cloud layer and liquid water contents are decreased quadratically up to 253 K.

11. Liquid water is included for cases mixed phases cases determined by 2B-CLDCLASS-LIDAR. Description of water partitioning can be found in Van Trict et al [20].

12. Aerosols optical properties modeled in 2B-FLXHR-LIDAR are taken from D'Almeida et al. [9] and WCP-55 [16] similar to the SPRINTARS global aerosol transport model (Takemura et al. [10]), which includes the asymmetry parameter and single scattering albedo. Smoke aerosol optical properties are constrained using data from the ORACLES field campaign Pistone et al. [10]. Mean optical propeties from a granule of data are found in Table 2. Aerosols above the boundary layer defined as polluted continental/smoke are given smoke-based aerosol optical properties. This assumption is consistent with the decisions made in CALIPSO V3 products.

13. Atmospheric profiles of water vapor, temperature, and Ozone in the algorithm are determined from ECMWF analyses (section 3.2.3).

14. Top-of-atmosphere variables are included as separate output variables. Seasonal values of water vapor, temperature, and Ozone are interpolated to values in each CloudSat profile to estimate fluxes up to 0.001 hPa (around 100 km).

15. Uniform mixing ratios of CO_2, CH_4 and N_2O are included with values of 400.0, 1.6, and 0.28 ppmv respectively.

16. After processing each orbit, 2B-FLXHR-LIDAR will also routinely compute top of the atmosphere (TOA) and surface (SFC) flux statistics for quality assessment purposes (see Section 7 for details).

Table 2: Example Aerosol Optical properties from a single granule.

Type	SSA	g
Marine	0.96	0.77
Dust	0.93	0.74
Polluted Dust	0.94	0.70
Clean Continental	0.99	0.74
Polluted Continental	0.99	0.76
Smoke	0.83	0.66
Dusty Marine	0.94	0.71

3 Algorithm Inputs to 2B-FLXHR-LIDAR

3.1 CloudSat Level 2 Products

3.1.1 2B-GEOPROF

Time and location for each CloudSat pixel are supplied by the CloudSat geometric profile product (2B-GEOPROF). Table 3 summarizes the appropriate variables and their properties (see Li and Durden [15] for more details).

Table 3: Inputs from 2B-GEOPROF (per profile)

Variable Name	Dimensions	Range	Units	Description
TAI_start	scalar	0 - 6×10^8	s	International Atomic Time at granule start
$Profile\_time$	scalar	0 - 86400	s	elapsed time since TIA_start
ray_lat	scalar	-90 - +90	deg	latitude
ray_lon	scalar	-180 - +180	deg	longitude
$Height$	vector (125)	-5000 - 30000	m	Height of each range bin
$nSurfaceBin$	scalar	1 - nbin	-	surface bin number

3.1.2 2B-CWC-RO

The 2B-FLXHR-LIDAR algorithm also requires complete profiles of cloud liquid water content and ice water content from the 2B-CWC product. 2B-CWC-RO is only used for radar-only estimates and are required along with appropriate quality control flags. 2B-CWC-RO also implicitly determines the vertical sampling interval for the output. A detailed description of these products and their sizes is provided in Table 4.

3.1.3 2C-PRECIP-COLUMN

In profiles where precipitation is present and the 2B-CWC fails to converge to an answer, 2C-PRECIP-COLUMN is used to input LWCs into 2B-FLXHR-LIDAR. Information from this product includes LWC for cloud and precipitation, height of liquid precipitation top, freezing level, and retrieval flags. More detail description of the product can be found in Table 5.

Table 4: Inputs from 2B_CWC (per profile)

Variable Name	Dimensions	Range	Units	Description
ro_lwc	vector (125)	0 - 10	g/m^3	radar-only cloud liquid water content
ro_iwc	vector (125)	0 - 1000	mg/m^3	radar-only cloud ice water content
ro_lre	vector (125)	0 - 1000	mg/m^3	radar-only liquid cloud effective radius
ro_ire	vector (125)	0 - 1000	mg/m^3	radar-only ice cloud effective radius
$icefrac$	scalar	0 - 1	–	Ice phase fraction
ro_status	scalar	0 - 20	–	Radar-only status flag

Table 5: Inputs from 2C-PRECIP-COLUMN (per profile)

Variable Name	Dimensions	Range	Units	Description
$Freezing\_Level$	scalar	0 - 10	km	Height of freezing level
$Rain\_Top$	scalar	0 - 18	km	Height of rain top
$Precip\_Flag$	scalar	0 - 9	-	Precipitation type
$Diagnostic\_retrieval\_info$	scalar	0 - 51	-	Status Flag

3.1.4   2B-CLDCLASS-LIDAR

To maintain consistency between cloud subtyping and phase classifcation cloud layers and their heights are identified through the combined CloudSat and CALIPSO product (2B-CLDCLASS-LIDAR). Table 6 summarizes the appropriate variables and their properties Wang and Sassen [22]).

Table 6: Inputs from 2B-CLDCLASS-LIDAR (per profile)

Variable Name	Dimensions	Range	Units	Description
$CloudFraction$	scalar	0 - 1	-	Fraction of lidar volumes containing hydrometeors per radar volume
$CloudLayers$	scalar	0 - 10	-	Number of cloud layers
$LayerBase$	vector(10)	0 - 20	m	Height of cloud base
$LayerTop$	vector(10)	0 -20	m	Height of cloud top
$CloudPhase$	vector(10)	0-3		Determine if cloud is ice, mixed, or liquid

3.1.5   2C-ICE

Ice properties for clouds detected only by CALIPSO are input from the combined CloudSat and CALIPSO ice product (2C-ICE). Table 7 summarizes the appropriate variables and their properties.

Table 7: Inputs from 2B-GEOPROF-LIDAR (per profile)

Variable Name	Dimensions	Range	Units	Description
Re	vector(125)	0 - 100	-	Ice effective radii
IWC	scalar	0 - 5	-	Ice water content

3.2 Ancillary Data Sets

3.2.1 MOD06-1KM-AUX

To more accurately calculate the properties of clouds undetected by CloudSat, 2B-FLXHR-LIDAR makes use of the MODIS based MOD06-1KM-AUX to obtain the optical depth and mean effective radius of single layer clouds. Variables of the MOD06-1KM-AUX product can be found in Table 8.

Table 8: Inputs from 2B-TAU (per profile)

Variable Name	Dimensions	Range	Units	Description
$Cloud\_Effective\_Radius$	scalar	0 - 100	micron	Mean effective radius for profile
$Cloud\_Optical\_Thickness$	scalar	0 - 100	-	Total optical depth for profile

3.2.2 CALIPSO Input

Information regarding clouds and aerosol detected only by CALIPSO are input into FLXHR-LIDAR-AUX. FLXHR-LIDAR-AUX is composed of collocated CALIPSO data from Version 4 CAL_LID_L2_05kmCLay and CAL_LID_L2_05kmALay products. The collocated data includes CALIPSO's aerosol optical depths, aerosol height, and aerosol type. Optical depths of thin cirrus are included using CALIPSO's optical depth as well as optical depth calculated by using a lidar-transmission method (described in Haladay et al. [7]) from the CALIPSO_L1B_ValStage1 data. Further description of the variables in the product can be found in Tables 9 and 10.

Table 9: Inputs from FLXHR-LIDAR-AUX (per profile)

Variable Name	Dimensions	Range	Units	Description
$Layer\_Type$	vector(5)	-	-	Distinguishes CloudSat and CALIPSO clouds
$CS\_Optical\_Depth$	scalar	0 - 5	-	Lidar-Transmission optical depth
$CAL\_Optical\_Depth$	vector (10)	0 - 5	-	CALIPSO cloud optical depth
$Alay\_Base$	vector (10)	0 - 25	km	Aerosol base height
$Alay\_Top$	vector (10)	0 - 25	km	Aerosol top height
$Alay\_Tau$	vector (10)	0-???	-	Optical depth of aerosol layer
$Alay\_Flag$	vector (125)	0-???	-	Aerosol description flags from VFM

Table 10: Inputs from CALIPSO_L1B_ValStage1-V4 (per profile)

Variable Name	Dimensions	Range	Units	Description
$Total\_Attenuated\_Backscatter\_532$	vector(583)	0 - 3.1	km^-1sr^-1	CALIOP Total Attenuated Backscatter at 532 nm
$Lidar\_Data\_Altitudes$	vector(583)	-2 - 40	km	Altitude of lidar measurement

3.2.3 Atmospheric State Variables

Atmospheric state variables describing the background atmospheric and surface properties are supplied to 2B-FLXHR-LIDAR by the CloudSat ECMWF-AUX data product. The ECMWF-AUX inputs required for the 2B-FLXHR-LIDAR algorithms consist of surface pressure, surface temperature, profiles of pressure, temperature, and specific humidity and are summarized in Table 11.

3.2.4 CloudSat Ancillary Albedo Dataset

In addition to the products listed above, the flux calculations require the reflection properties of the underlying surface to be specified. For this purpose, 2B-FLXHR-LIDAR require surface albedo estimates in the visible and near-infrared spectral bands from the CloudSat ancillary albedo product, AN-ALBEDO. Table 12 summarizes the variables required.

Table 11: Inputs from ECMWF-AUX (per profile)

Variable Name	Dimensions	Range	Units	Description
T_{sfc}	scalar	150-350	K	surface temperature
P	vector (125)	$0 - 1.02\times10^5$	Pa	pressure
T	vector (125)	150-350	K	temperature
q_v	vector (125)	0.00 - 1.00	kg/kg	specific humidity
O_3	vector (125)	0-???	ppm	Ozone mixing ratio

Table 12: Inputs from AN-ALBEDO (per profile)

Variable Name	Dimensions	Range	Units	Description
$A_{s,v}$	scalar	0. - 1.	–	visible surface albedo
$A_{s,nir}$	scalar	0. - 1.	–	near-IR surface albedo

3.2.5 Ice and Snow from the Near-real-time Ice and Snow Extent (NISE) data set

The variability of sea ice is obtained in real time from NISE data set. Surface characteristics are described in Table 13.

Table 13: Inputs from MOD06-1KM-AUX (per profile)

Variable Name	Dimensions	Range	Units	Description
Age	scalar		-	Time since last observation
$Extent$	scalar		-	Snow coverage and sea ice concentration

3.2.6 Ancillary MODIS Data

The solar zenith angle supplied by the MODIS-AUX data product. Details concerning the MODIS-AUX solar zenith angle are summarized in Table 14.

Table 14: Algorithm Parameters (per profile)

Variable Name	Dimensions	Range	Units	Description
SZA	scalar	0. - 180.	degrees	solar zenith angle

3.3 Control and Calibration

At present no calibration of the algorithms is planned. As a result, no ancillary control or calibration data is required. See Section 4.3.2 for details regarding planned validation activities for the 2B-FLXHR-LIDAR products.

4 Algorithm Summary

4.1 Pseudo-code

The following provides a pseudo-code description outlining the details of the steps in the algorithm flow diagram in Figure 1:

start 2B-FLXHR-LIDAR

open 2B-GEOPROF

open 2B-CLDCLASS-LIDAR

open 2B-CWC-RO

open MOD06-1KM-AUX

open 2C-PRECIP-COLUMN

open 2C-ICE

open FLXHR-LIDAR-AUX

open NISE

open ECMWF-AUX

open 2B-FLXHR-LIDAR output file

open albedo ancillary data file (AN-ALBEDO)

set top-of-atmosphere, beam-normal irradiance F_0

for-each profile

> **read** ray number r (2B-GEOPROF)
>
> **get** time t (2B-GEOPROF)
>
> **get** geometry parameters lat, $nSurfaceBin$ (2B-GEOPROF)
>
> **compute** solar zenith angle (SZA), orbital eccentricity factor
>
> **read** cloud liquid and ice water contents (2B-CWC-RO)
>
> **get** CALIPSO cloud and aerosol (FLXHR-LIDAR-AUX;2B-CLDCLASS-LIDAR)
>
> **compute** Check cloud boundaries (2B-CLDCLASS-LIDAR)
>
> **compute** Check cloud phase (2B-CLDCLASS-LIDAR)
>
> **compute** aerosol optical properties
>
> **read** MODIS cloud properties (MOD06-1KM-AUX)
>
> **compute** LWC and IWC of undetected clouds
>
> **compute** LWC and IWC of flagged CWC-RO cases
>
> **read** precipitation liquid water contents (2C-PRECIP-COLOMN)
>
> **compute** LWC and IWC of flagged raining cases
>
> **read** atmosphere state variables (ECMWF-AUX)
>
> **read** surface albedos (AN-ALBEDO)
>
> **read** NISE surface characteristics (NISE)
>
> **compute** fluxes and heating rates

end-for-each profile

compute scale factors, offsets

compute scaled fluxes and heating rates

compute latitude-mean flux and heating rate statistics

write scale factors, offsets

write scaled fluxes, heating rates

write latitude-mean flux and heating rate statistics

close 2B-FLXHR-LIDAR output file

close AN-ALBEDO

close 2B-CWC

close MOD06-1KM-AUX

close 2C-PRECIP-COLUMN

close 2C-ICE

close FLXHR-LIDAR-AUX

close NISE

close ECMWF-AUX

close 2B-CLDCLASS-LIDAR

close 2B-GEOPROF

stop 2B-FLXHR-LIDAR

4.2 Algorithm Parameters

In addition to the input variables listed in Section 3, a number of parameters are set in the 2B-FLXHR-LIDAR algorithms. These are summarized in Table 15.

Table 15: Algorithm Parameters (per profile)

Variable Name	Dimensions	Range	Units	Description
F_0	scalar	1500	$Wm^{-2}\mu m^{-1}$	TOA incident, beam-normal irradiance
e	scalar	0. - 1.	–	orbital eccentricity factor
rel	scalar	13.	μm	liquid cloud effective radius[1]
rei	scalar	30.	μm	ice cloud effective radius[1]
$wpfill$	scalar	TBD	kgm^3	water path fill value[2]
$ipfill$	scalar	TBD	kgm^3	ice path fill value[2]
$asys$	scalar	0. - 1.	–	aerosol asymmetry parameter
$waer$	scalar	0. - 1.	–	aerosol single scattering albedo
$[CO_2]$	scalar	300. - 400.	ppmv	carbon dioxide concentration
$[CH_4]$	scalar	TBD	ppmv	methane concentration
$[N_2O]$	scalar	TBD	ppmv	nitrous oxide concentration

4.3 Algorithm Performance

4.3.1 Timing Requirements and Performance

As retrievals are to be performed in real time, the requirement on the computational speed of the algorithm is estimated from the following considerations:

- satellite speed along ground track $\sim$7 km s^{-1}

- 3.5 km resolution along-track

This yields approximately two pixels to process per second allowing a half second per pixel, in the absence of additional constraints. However, since the algorithm requires inputs from a number of other CloudSat products to run their processing time must be factored in to the calculation. Based on estimates of the processing times for the 2B-GEOPROF and 2B-CWC algorithms, we impose a maximum processing time of 0.05-0.1 seconds per ray.

4.3.2   Uncertainty Requirements and Performance

The specific goals for the quality of the 2B-FLXHR-LIDAR flux and heating rate products as laid out in the CloudSat Step-2 ESSP-2 Proposal are as follows:

- Atmospheric fluxes at 500m resolution accurate to 5 Wm^{-2}.

- Atmospheric heating rates at 500m resolution accurate to 1 Kday^{-1}.

The evaluation of the original radar only 2B-FLXHR can be found in (L'Ecuyer et al. [8]). Detailed evaluation of 2B-FLXHR-LIDAR product and related uncertainties can be found in Henderson et al [16] and Matus et al [18] Validation of mixed-phased properties are reported in McIllhatten et al [19] and Van Trict et al [20]. Aerosol uncertainty is addressed in Henderson et al [16] and using the new R05 2B-FLXHR-LIDAR data in Matus et al [17]. A summary of the approach used to validate is described below.

Aquiring the aforementioned validation goals can be considered as a two-pronged approach consisting of both verification of the inputs to the algorithm as well as more traditional validation of the output. This approach not only evaluates the performance of the algorithm for comparison to the mission requirements but also provides a unique opportunity to study the contributions of various sources of error to the overall uncertainty in the product.

The verification of algorithm inputs is largely covered as part of the validation plans for the other CloudSat products up the level 2 chain. Uncertainties in the 2B-CWC products, for example, will be provided by their respective algorithm teams after launch and the uncertainties in the atmospheric state variables from the ECMWF-AUX and AN-ALBEDO datasets will be obtained from their sources. Using these error estimates, a series of sensitivity studies will be conducted using an offline version of 2B-FLXHR-LIDAR algorithm and a subset of the CloudSat observations. The results will provide bounds on the expected uncertainties in the flux and heating rate products due to errors in all algorithm inputs and will serve as an initial evaluation of algorithm performance.

To supplement these sensitivity studies, flux observations/estimates from the Clouds and the Earth's Radiant Energy System (CERES) aboard Aqua will also be compared with the 2B-FLXHR-LIDAR products. The CERES instrument provides estimates of outgoing longwave and shortwave radiation at the top of the atmosphere and, through independent algorithms, the CERES team infer longwave and shortwave fluxes at the Earth's surface. Both will be compared with CloudSat products on a range of temporal and spatial scales. While these comparisons are restricted to fluxes at the atmospheric boundaries (i.e. the top of the atmosphere and the surface) they will serve to verify the uncertainty estimates derived through the above sensitivity studies providing a more complete analysis of the algorithm's performance characteristics. A combination of the results obtained from each of these evaluation approaches will ultimately be compared to the requirements above to assess its overall performance in the context of the mission as a whole.

5   Data Product Output Format

5.1   Data Contents

To provide status information about the fluxes and heating rates estimates by the 2B-FLXHR-LIDAR algorithm, each pixel is assigned status flags providing additional information pertaining to the output.

The scene status flag is indicates whether or not the external products are used in any given pixel. The flag will indicate day/night, precipitating clouds, cloud and aerosol detected by CALIPSO, if 2B-CWC data were constrained using visible optical depth information from MOD06-1KM-AUX, sea ice, and missing/bad data.The flagging system uses a 16-bit flag with values for each bit flag summarized in Table 17. A value of 1 corresponds to True.

Also included is the status flag, which describes the generic cases found in each profile. This includes all clouds detected by the radar or lidar. In this flag each pixel will also be assigned a status flag with a value between 1 and 20 that will identify the cloud type or types present in the scene as well as indicating scenes in which drizzle may have contaminated the 2B-CWC product. Table 17 provides a summary of all status flags used by 2B-FLXHR-LIDAR. Note that all pixels with flag values of eight or less should contain valid flux and heating rate output while flags greater than this value will generally be filled with missing values. Flags 5-7 are all indicative of possible precipitation within the CloudSat footprint. In cases where the CWC algorithm was able to converge on a solution, it was used to specify liquid and ice water contents. Flag values of 6 or 7 indicate cases where the CWC liquid or ice water content algorithms failed, respectively, and fill values were assumed for the appropriate water contents (see steps 6-11 in Section 2.2.2).

A new lidar flag is indicates additional information provided by 2B-CLDCLASS-LIDAR. The flagging system uses a 8-bit flag with values for each bit flag summarized in Table 18. A value of 1 corresponds to True.

Table 16: Values for scene status flag.

Bit	Meaning
01	Daytime pixel
02	Non-precipitation cloud
03	Precipitation present
04	CALIOP high cloud
05	CALIOP + MODIS low cloud
06	CALIOP-only low cloud
07	CALIOP aerosol
08	NISE Sea Ice
09	Bad surface bin
10	High uncertainty in CWC
11	Missing CWC
12	CWC-RO possible precipitaiton
13	Missing CALIOP
14	Missing MODIS
15	Missing NISE
16	Out-of-Bounds Flux

Table 17: Values for flux and heating rate status flag.

Value	Meaning
01	Clear pixel
02	Only a liquid cloud present
03	Only an ice cloud present
04	Both types of non-precipitating cloud present
05	Possible drizzle/precipitation
06	Filled LWC due to missing cloud or precipitation
07	Filled IWC due to missing cloud or precipitation
08	High χ^2 in either LWC or IWC retrieval
09	Bad LWC input data (see 2B-CWC for explanation)
10	Bad IWC input data (see 2B-CWC for explanation)
17	Bad surface bin in 2B-GEOPROF
18	Bad MODIS-AUX input data
19	Out-of-bounds flux encountered

Table 18: Values for lidar status flag.

Bit	Meaning
01	CALIPSO cloud detected
02	Ice cloud above 4km
03	Ice cloud below 4km
04	Liquid cloud above 4km
05	Liquid cloud below 4km
06	Mixed-phase cloud above 4km
07	Mixed-phase cloud below 4km
08	Missing 2B-CLDCLASS-LIDAR

Among the expected uses for CloudSat flux and heating rate data is to provide a source of information for analyzing global and regional radiation budgets. To this end, the 2B-FLXHR-LIDAR algorithms will also provide mean fluxes at

the top of the atmosphere (TOA) and surface (SFC) and mean column-integrated radiative heating rates spatially averaged over both the full CloudSat domain and various latitude belts ranging from the tropics to the high latitudes. The particular latitude belts chosen for the 2B-FLXHR-LIDAR algorithms and appropriate physical interpretations are summarized in Table 19. For each of these regions, the 2B-FLXHR-LIDAR algorithms will provide the mean and standard deviation of

Table 19: Latitude ranges over which statistics will be computed.

Name	Range
Orbit	The entire CloudSat orbit
North High Latitudes	55 N to 90 N
North Midlatitudes	35 N to 55 N
North Subtropics	23.5 N to 35 N
Tropics	23.5 S to 23.5 N
South Subtropics	23.5 S to 35 S
South Midlatitudes	35 S to 55 S
South High Latitudes	55 S to 90 S

upwelling and downwelling longwave and shortwave fluxes at both TOA and SFC over each orbit. The mean and standard deviation of the estimated column-integrated longwave and shortwave radiative heating will also be computed and stored.

All of these 2B-FLXHR-LIDAR data products are summarized in Table 20. The parameter "nz" is the total number of vertical intervals at which data are reported, typically 125, and the parameter "nb" is the number of bands for which data are reported, in this case two. "nray" is the total number of profiles in the data granule, "nflags" is the total number of pixel status flags that may be assigned, and "nlatbins" is the number of latitude bins for which TOA and SFC flux statistics are produced.

Table 20: Algorithm Outputs

Variable Name	Dimensions	Range	Units	Description
$FD_{\lambda,z}$	nray*nz*nb vector	0 .- 1500.	Wm^{-2}	downwelling flux
$FD\_NC_{\lambda,z}$	nray*nz*nb vector	0 .- 1500.	Wm^{-2}	downwelling flux with no cloud
$FD\_NA_{\lambda,z}**$	nray*nz*nb vector	0 .- 1500.	Wm^{-2}	downwelling flux with no aerosol
$FD\_TOA\_IncomingSolar_{\lambda,z}$	nray*nb vector	0 .- 1500.	Wm^{-2}	downwelling flux at top-of-atmosphere only
$FU_{\lambda,z}$	nray*nz*nb vector	0 .- 1500.	Wm^{-2}	upwelling flux
$FU\_NC_{\lambda,z}$	nray*nz*nb vector	0 .- 1500.	Wm^{-2}	upwelling flux with no cloud
$FU\_NA_{\lambda,z}**$	nray*nz*nb vector	0 .- 1500.	Wm^{-2}	upwelling flux with no aerosol
$FU\_TOA_{\lambda,z}$	nray*nb vector	0 .- 1500.	Wm^{-2}	upwelling flux at top-of-atmosphere only
$FU\_NC\_TOA_{\lambda,z}$	nray*nb vector	0 .- 1500.	Wm^{-2}	upwelling flux with no cloud at top-of-atmosphere only
$FU\_NA\_TOA_{\lambda,z}**$	nray*nb vector	0 .- 1500.	Wm^{-2}	upwelling flux with no aerosol at top-of-atmosphere only
$TOACRE_{\lambda}$	nray*nb vector	0 .- 1500.	Wm^{-2}	Top-of-atmosphere cloud radiative effect
$BOACRE_{\lambda}$	nray*nb vector	0 .- 1500.	Wm^{-2}	Bottom-of-atmosphere cloud radiative effect
$QR_{\lambda\,z}$	nray*nz*(nb-1) vector	-200. - 200.	K day^{-1}	heating rate
COD	nray*nz*nb vector	–	–	vertically resolved cloud optical depth
Scene_Status	nray scalar	0 - 1	–	bit-based scene status flag for added cloud and data
Status	nray scalar	1 - 20	–	general pixel status flag
Lidar_Status	nray scalar	0-1	–	bit-based flag used for lidar-based properties and cwc-ro precip
Land_Char	nray scalar	1 - 18	–	IGBP/NISE land characteristic
Albedo	nray scalar	0 - 100	–	Surface albedo
BinCounts	nflags*nlatbins vector	0 - nray	–	Number of pixels in each lat/status bin
Meansolar	nflags*nlatbins vector	0 - 1500	Wm^{-2}	mean solar insolation
Sigmasolar	nflags*nlatbins vector	0 - 1500	Wm^{-2}	standard deviation of solar insolation
MeanOSR	nflags*nlatbins vector	0 - 1500	Wm^{-2}	mean OSR
SigmaOSR	nflags*nlatbins vector	0 - 1500	Wm^{-2}	standard deviation of OSR
MeanSSR	nflags*nlatbins vector	0 - 1500	Wm^{-2}	mean SSR
SigmaSSR	nflags*nlatbins vector	0 - 1500	Wm^{-2}	standard deviation of SSR
MeanSFCR	nflags*nlatbins vector	0 - 1500	Wm^{-2}	mean surface reflection
SigmaSFCR	nflags*nlatbins vector	0 - 1500	Wm^{-2}	standard deviation of surface reflection
MeanOLR	nflags*nlatbins vector	0 - 1500	Wm^{-2}	mean OLR
SigmaOLR	nflags*nlatbins vector	0 - 1500	Wm^{-2}	standard deviation of OLR
MeanSLR	nflags*nlatbins vector	0 - 1500	Wm^{-2}	mean SLR
SigmaSLR	nflags*nlatbins vector	0 - 1500	Wm^{-2}	standard deviation of SLR
MeanSFCE	nflags*nlatbins vector	0 - 1500	Wm^{-2}	mean surface emission
SigmaSFCE	nflags*nlatbins vector	0 - 1500	Wm^{-2}	standard deviation of surface emission
MeanQLW	nflags*nlatbins vector	-10 - 10	K day^{-1}	mean atmospheric longwave heating
SigmaQLW	nflags*nlatbins vector	-10 - 10	K day^{-1}	standard deviation of atmospheric longwave heating
MeanQSW	nflags*nlatbins vector	-10 - 10	K day^{-1}	mean atmospheric shortwave heating
SigmaQSW	nflags*nlatbins vector	-10 - 10	K day^{-1}	standard deviation of atmospheric shortwave heating

5.2   Data Format Overview

In addition to the data specific to the 2B-FLXHR-LIDAR algorithm results, the HDF-EOS data structure may incorporate granule data/metadata (describing the characteristics of the orbit or granule) and supplementary ray data/metadata. The data structure is described in Table 21. Only those data fields specifically required by the 2B-FLXHR-LIDAR algorithms are listed in the table and included in the descriptions in Section 5.3. The entries in the "Size" column of the table represent the array size where appropriate (*e.g.*, nray), the variable type (REAL, INTEGER, CHAR) and the size in bytes of each element (*e.g.*, (4)). The parameter "nray" is the total number of profiles in the granule.

Table 21: HDF-EOS File Structure

		Structure/Data Name		Size
Data	Swath	Common metadata	TBD	TBD
Granule	Metadata	2B-FLXHR-LIDAR metadata	$F_{\lambda z}$ scale factor	REAL(4)
			$F_{\lambda z}$ offset	REAL(4)
			$QR_{\lambda z}$ scale factor	REAL(4)
			$QR_{\lambda z}$ offset	REAL(4)
			BF scale factor	REAL(4)
			BF offset	REAL(4)
			BQR scale factor	REAL(4)
			BQR offset	REAL(4)
			Flag counts	nflags*INT(2)
	Swath	Common data fields	Time	nray*REAL(8)
			Status flag	nray*INTEGER(2)
			Geolocation latitude	nray*REAL(4)
			Surface bin number	nray*INT(2)
		2B-FLXHR-LIDAR	$FD_{\lambda z}$	nz*nb*nray*INTEGER(2)
		pixel data	$FD\_TOA\_IncomingSolar_{\lambda z}$	nb*nray*INTEGER(2)
			$FD\_NC_{\lambda z}$	nz*nb*nray*INTEGER(2)
			$FD\_NA_{\lambda z}$	nz*nb*nray*INTEGER(2)
			$FU_{\lambda z}$	nz*nb*nray*INTEGER(2)
			$FU\_NC_{\lambda z}$	nz*nb*nray*INTEGER(2)
			$FU\_NA_{\lambda z}$	nz*nb*nray*INTEGER(2)
			$FU\_TOA_{\lambda z}$	nb*nray*INTEGER(2)
			$FU\_NC\_TOA_{\lambda z}$	nb*nray*INTEGER(2)
			$FU\_NA\_TOA_{\lambda z}$	nb*nray*INTEGER(2)
			$COD_{\lambda z}$	nz*nb*nray*INTEGER(2)
			$QR_{\lambda z}$	nz*(nb-1)*nray*INTEGER(2)
			TOACRE	nray*INTEGER(2)
			BOACRE	nray*INTEGER(2)
			Scene_Status	nray*UINTEGER(2)
			Status	nray*INTEGER(2)
			Lidar_Status	nray*UINTEGER(2)
			Land_Char	nray*INTEGER(2)
			Albedo	nray*INTEGER(2)
		2B-FLXHR-LIDAR	BinCounts	nlatbins*nflags*INTEGER(2)
		orbit data	Meansolar	nlatbins*nflags*INTEGER(2)
			Sigmasolar	nlatbins*nflags*INTEGER(2)
			MeanOSR	nlatbins*nflags*INTEGER(2)
			SigmaOSR	nlatbins*nflags*INTEGER(2)
			MeanSSR	nlatbins*nflags*INTEGER(2)
			SigmaSSR	nlatbins*nflags*INTEGER(2)
			MeanSFCR	nlatbins*nflags*INTEGER(2)
			SigmaSFCR	nlatbins*nflags*INTEGER(2)
			MeanOLR	nlatbins*nflags*INTEGER(2)
			SigmaOLR	nlatbins*nflags*INTEGER(2)
			MeanSLR	nlatbins*nflags*INTEGER(2)
			SigmaSLR	nlatbins*nflags*INTEGER(2)
			MeanSFCE	nlatbins*nflags*INTEGER(2)
			SigmaSFCE	nlatbins*nflags*INTEGER(2)
			MeanQSW	nlatbins*nflags*INTEGER(2)
			SigmaQSW	nlatbins*nflags*INTEGER(2)
			MeanQLW	nlatbins*nflags*INTEGER(2)
			SigmaQLW	nlatbins*nflags*INTEGER(2)

5.3   Data Descriptions

2B-FLXHR and 2B-FLXHR-LIDAR data fields:

FD$_{\lambda z}$ (SDS, nz*nb*nray*INTEGER(2))
Band-integrated downwelling flux profile estimates. Shortwave estimates are stored as the first element followed by the longwave estimates. All values range from 0 to 1500 and are stored as two-byte integers with All values are multiplied by 10. The fill value -999 corresponds to bad/missing input or out-of-bounds fluxes.

FD_NC$_{\lambda z}$ (SDS, nz*nb*nray*INTEGER(2))
Band-integrated downwelling flux profile estimates for cloud-cleared skies. These estimates assume identical atmospheric and surface properties as $FD_{\lambda z}$ but all cloud water contents are set to zero. Shortwave estimates are stored as the first element followed by the longwave estimates. All values range from 0 to 1500 and are stored as two-byte integers with All values are multiplied by 10. The fill value -999 corresponds to bad/missing input or out-of-bounds fluxes.

FD_TOA_IncomingSolar$_{\lambda z}$ (SDS, nray*INTEGER(2))
Band-integrated downwelling flux estimates only at top-of-atmosphere for incoming solar radiation. All values range from 0 to 1500 and are stored as two-byte integers with All values are multiplied by 10. The fill value -999 corresponds to bad/missing input or out-of-bounds fluxes.

FD_NA$_{\lambda z}$ ** (SDS, nz*nb*nray*INTEGER(2))
Band-integrated downwelling flux profile estimates skies with no aerosol included. These estimates assume identical atmospheric and surface properties as $FD_{\lambda z}$ but all aerosol contents are set to zero. Shortwave estimates are stored as the first element followed by the longwave estimates. All values range from 0 to 1500 and are stored as two-byte integers with All values are multiplied by 10. The fill value -999 corresponds to bad/missing input or out-of-bounds fluxes.

FU$_{\lambda z}$ (SDS, nz*nb*nray*INTEGER(2))
Band-integrated upwelling flux profile estimates. Shortwave estimates are stored as the first element followed by the longwave estimates. All values range from 0 to 1500 and are stored as two-byte integers with All values are multiplied by 10. The fill value -999 corresponds to bad/missing input or out-of-bounds fluxes.

FU_NC$_{\lambda z}$ (SDS, nz*nb*nray*INTEGER(2))
Band-integrated upwelling flux profile estimates for cloud-cleared skies. These estimates assume identical atmospheric and surface properties as $FD_{\lambda z}$ but all cloud water contents are set to zero. Shortwave estimates are stored as the first element followed by the longwave estimates. All values range from 0 to 1500 and are stored as two-byte integers with All values are multiplied by 10. The fill value -999 corresponds to bad/missing input or out-of-bounds fluxes.

FU_NA$_{\lambda z}$ ** (SDS, nz*nb*nray*INTEGER(2))
Band-integrated upwelling flux profile estimates skies with no aerosol included. These estimates assume identical atmospheric and surface properties as $FU_{\lambda z}$ but all aerosol contents are set to zero. Shortwave estimates are stored as the first element followed by the longwave estimates. All values range from 0 to 1500 and are stored as two-byte integers with All values are multiplied by 10. The fill value -999 corresponds to bad/missing input or out-of-bounds fluxes.

FU_TOA$_{\lambda z}$ (SDS, nb*nray*INTEGER(2))
Band-integrated upwelling flux estimates only at the top-of-atmosphere. Shortwave estimates are stored as the first element followed by the longwave estimates. All values range from 0 to 1500 and are stored as two-byte integers with All values are multiplied by 10. The fill value -999 corresponds to bad/missing input or out-of-bounds fluxes.

FU_NC_TOA$_{\lambda z}$ (SDS, nb*nray*INTEGER(2))
Band-integrated upwelling flux estimates for cloud-cleared skies only at the top-of-atmosphere. These estimates assume identical atmospheric and surface properties as $FD_{\lambda z}$ but all cloud water contents are set to zero. Shortwave estimates are stored as the first element followed by the longwave estimates. All values range from 0 to 1500 and are stored as two-byte integers with All values are multiplied by 10. The fill value -999 corresponds to bad/missing input or out-of-bounds fluxes.

FU_NA_TOA$_{\lambda z}$ ** (SDS, nb*nray*INTEGER(2))
Band-integrated upwelling flux estimates skies with no aerosol included only at the top-of-atmosphere. These

estimates assume identical atmospheric and surface properties as $FU_{\lambda z}$ but all aerosol contents are set to zero. Shortwave estimates are stored as the first element followed by the longwave estimates. All values range from 0 to 1500 and are stored as two-byte integers with All values are multiplied by 10. The fill value -999 corresponds to bad/missing input or out-of-bounds fluxes.

QR$_{\lambda z}$ (SDS, nz*nb*nray*INTEGER(2))

Band-integrated heating rate estimates. Shortwave estimates are stored as the first element followed by the longwave estimates. All values are multiplied by 100 and stored as two-byte integers. Prior to adjustment all values fall between -200 and 200 K d^{-1}. The fill value -999 corresponds to bad/missing input or out-of-bounds fluxes.

COD$_{\lambda z}$ (SDS, nz*nb*nray*INTEGER(2))

Single band SW (Band: 0.20-0.69) and LW (Band: 10.20-12.50) vertically resolved cloud optical depth. Shortwave estimates are stored as the first element followed by the longwave estimates. All values are multiplied by 1000 and stored as two-byte integers. The fill value -999 corresponds to bad/missing inputs.

TOACRE$_{\lambda}$ (SDS, nray*INTEGER(2))

Top of the atmosphere cloud radiative effect (also referred to as cloud 'forcing'). Shortwave estimates are stored as the first element followed by the longwave estimates. All values range from 0 to 1500 and are stored as two-byte integers.

BOACRE$_{\lambda}$ (SDS, nray*INTEGER(2))

Bottom of the atmosphere (i.e. surface) cloud radiative effect (also referred to as cloud 'forcing'). Shortwave estimates are stored as the first element followed by the longwave estimates. All values range from 0 to 1500 and are stored as two-byte integers.

Scene_Status (SDS, nray*UINTEGER(2))

A 16-byte binary flag with bits allocated according to Table 17. This flag includes indicators of the presence of clouds, precipitation, and aerosol. The flag also includes information regarding the status of input data into the algorithms.

Status (SDS, nray*INTEGER(2))

A two-byte integer quality control flag with bits allocated according to Table 17. This flag includes indicators of bad input data, bad flux data, drizzle, etc.

Lidar_Status (SDS, nray*UINTEGER(2))

A 16-byte binary flag with bits allocated according to Table 18. This flag includes indicators of the presence of lidar clouds, phase and cwc-ro possible precipitation.

Land_Char (SDS, nray*INTEGER(2))

A two-byte integer containing land characteristics according to IGBP. Sea ice may be altered if NISE provides sea ice over oceans.

Albedo (SDS, nray*INTEGER(2))

A two-byte integer of the surface albedo in the visible (0.65 um)

BinCounts (SDS, nlatbins*nflags*INTEGER(2))

Number of pixels in orbit accumulated in each latitude band and status flag bin. All values range from 0 to "nray" and are stored as two-byte integers. The latitude bands over which statistics will be compiled are summarized in Table 19.

Meansolar (SDS, nlatbins*nflags*INTEGER(2))

Mean downwelling shortwave flux at the top of the atmosphere over each latitude band and status flag bin. All values range from 0 to 1500 and are stored as two-byte integers. The latitude bands over which statistics will be computed are summarized in Table 19.

Sigmasolar (SDS, nlatbins*nflags*INTEGER(2))

Standard deviation of downwelling shortwave flux at the surface over each latitude band and status flag bin. All values range from 0 to 1500 and are stored as two-byte integers. The latitude bands over which statistics will be computed are summarized in Table 19.

MeanOSR (SDS, nlatbins*nflags*INTEGER(2))

Mean upwelling shortwave flux at the top of the atmosphere, or outgoing shortwave radiation (OSR), over each latitude band and status flag bin. All values range from 0 to 1500 and are stored as two-byte integers. The latitude bands over which statistics will be computed are summarized in Table 19.

SigmaOSR (SDS, nlatbins*nflags*INTEGER(2))

Standard deviation of upwelling shortwave flux at the top of the atmosphere, or outgoing shortwave radiation (OSR), over each latitude band and status flag bin. All values range from 0 to 1500 and are stored as two-byte integers. The latitude bands over which statistics will be computed are summarized in Table 19.

MeanSSR (SDS, nlatbins*nflags*INTEGER(2))

Mean downwelling shortwave flux at the surface, or surface shortwave radiation (SSR), over each latitude band and status flag bin. All values range from 0 to 1500 and are stored as two-byte integers. The latitude bands over which statistics will be computed are summarized in Table 19.

SigmaSSR (SDS, nlatbins*nflags*INTEGER(2))

Standard deviation of downwelling shortwave flux at the surface, or surface shortwave radiation (SSR), over each latitude band and status flag bin. All values range from 0 to 1500 and are stored as two-byte integers. The latitude bands over which statistics will be computed are summarized in Table 19.

MeanSFCR (SDS, nlatbins*nflags*INTEGER(2))

Mean upwelling, or reflected, shortwave flux at the surface over each latitude band and status flag bin. All values range from 0 to 1500 and are stored as two-byte integers. The latitude bands over which statistics will be computed are summarized in Table 19.

SigmaSFCR (SDS, nlatbins*nflags*INTEGER(2))

Standard deviation of upwelling, or reflected, shortwave flux at the surface over each latitude band and status flag bin. All values range from 0 to 1500 and are stored as two-byte integers. The latitude bands over which statistics will be computed are summarized in Table 19.

MeanOLR (SDS, nlatbins*nflags*INTEGER(2))

Mean upwelling longwave flux at the top of the atmosphere, or outgoing longwave radiation (OLR), over each latitude band and status flag bin. All values range from 0 to 1500 and are stored as two-byte integers. The latitude bands over which statistics will be computed are summarized in Table 19.

SigmaOLR (SDS, nlatbins*nflags*INTEGER(2))

Standard deviation of upwelling longwave flux at the top of the atmosphere, or outgoing longwave radiation (OLR), over each latitude band and status flag bin. All values range from 0 to 1500 and are stored as two-byte integers. The latitude bands over which statistics will be computed are summarized in Table 19.

MeanSLR (SDS, nlatbins*nflags*INTEGER(2))

Mean downwelling longwave flux at the surface, or surface longwave radiation (SLR), over each latitude band and status flag bin. All values range from 0 to 1500 and are stored as two-byte integers. The latitude bands over which statistics will be computed are summarized in Table 19.

SigmaSLR (SDS, nlatbins*nflags*INTEGER(2))

Standard deviation of downwelling longwave flux at the surface, or surface longwave radiation (SLR), over each latitude band and status flag bin. All values range from 0 to 1500 and are stored as two-byte integers. The latitude bands over which statistics will be computed are summarized in Table 19.

MeanSFCE (SDS, nlatbins*nflags*INTEGER(2))

Mean upwelling, or emitted, longwave flux at the surface over each latitude band and status flag bin. All values range from 0 to 1500 and are stored as two-byte integers. The latitude bands over which statistics will be computed are summarized in Table 19.

SigmaSFCE (SDS, nlatbins*nflags*INTEGER(2))

Standard deviation of upwelling, or emitted, longwave flux at the surface over each latitude band and status flag bin. All values range from 0 to 1500 and are stored as two-byte integers. The latitude bands over which statistics will be computed are summarized in Table 19.

MeanQSW (SDS, nlatbins*nflags*INTEGER(2))

Mean total atmospheric shortwave heating over each latitude band and status flag bin. All values are multiplied by 100 and stored as two-byte integers. Prior to adjustment all values range from -10 to 10. The latitude bands over which statistics will be computed are summarized in Table 19.

SigmaQSW (SDS, nlatbins*nflags*INTEGER(2))

Standard deviation of total atmospheric shortwave heating over each latitude band and status flag bin. All values are multiplied by 100 and stored as two-byte integers. Prior to adjustment, all values range from -10 to 10. The latitude bands over which statistics will be computed are summarized in Table 19.

MeanQLW (SDS, nlatbins*nflags*INTEGER(2))

Mean total atmospheric longwave heating over each latitude band and status flag bin. All values are multiplied by 100 and stored as two-byte integers. Prior to adjustment, all values range from -10 to 10. The latitude bands over which statistics will be computed are summarized in Table 19.

SigmaQLW (SDS, nlatbins*nflags*INTEGER(2))

Standard deviation of total atmospheric longwave heating over each latitude band and status flag bin. All values are multiplied by 100 and stored as two-byte integers. Prior to adjustment, all values range from -10 to 10. The latitude bands over which statistics will be computed are summarized in Table 19.

** Denotes variable only reported in 2B-FLXHR-LIDAR

2B-FLXHR-LIDAR metadata fields:

$F_{\lambda z}$ **scale factor** (SDS attribute, REAL(4))

Scale factor used to rescale pixel-level fluxes, $FU_{\lambda z}$, $FD_{\lambda z}$, $FU\_NC_{\lambda z}$, $FD\_NC_{\lambda z}$ $FU\_NA_{\lambda z}$, and $FD\_NA_{\lambda z}$ as well as cloud forcings TOACRE$_\lambda$ and BOACRE$_\lambda$.

$F_{\lambda z}$ **offset** (SDS attribute, REAL(4))

Offset added to pixel-level fluxes, $FU_{\lambda z}$, $FD_{\lambda z}$, $FUclr_{\lambda z}$, and $FDclr_{\lambda z}$ as well as cloud forcings TOACRE$_\lambda$ and BOACRE$_\lambda$.

$QR_{\lambda z}$ **scale factor** (SDS attribute, REAL(4))

Scale factor used to rescale pixel-level radiative heating rates.

$QR_{\lambda z}$ **offset** (SDS attribute, REAL(4))

Offset added to pixel-level radiative heating rates.

BF scale factor (SDS attribute, REAL(4))

Scale factor used to rescale bin-mean (and standard deviation) fluxes.

BF offset (SDS attribute, REAL(4))

Offset added to bin-mean (and standard deviation) fluxes.

BQR scale factor (SDS attribute, REAL(4))

Scale factor used to rescale bin-mean (and standard deviation) radiative heating rates.

BQR offset (SDS attribute, REAL(4))

Offset added to bin-mean (and standard deviation) radiative heating rates.

Flag counts (SDS attribute, nflags*INT(2))

Granule status flag statistics providing the number of pixels along the orbit that are assigned each of the values described in Table 17 in the form of a 2-byte integer.

Common data fields:

time (nray*REAL(8))

Frame (or ray) international atomic time. Seconds since 00:00:00 1 Jan 1993.

geolocation latitude (nray*REAL(4))

The latitude of the center of the IFOV at the altitude of the earth ellipsoid (Li and Durden [15]).

Surface bin number (nray*INT(2))

Index of radar range bin coincident with earth' surface.

Common metadata_fields:

No additional metatdata are specifically required by 2B-FLXHR-LIDAR algorithm.

6   Examples

6.1   Product heating rate example

Input variables into 2B-FLXHR-LIDAR are illustrated in Figure 2. Also, sample heating rates from the 2B-FLXHR-LIDAR product for a small segment of CloudSat orbit 03616 are presented in Figure 3.
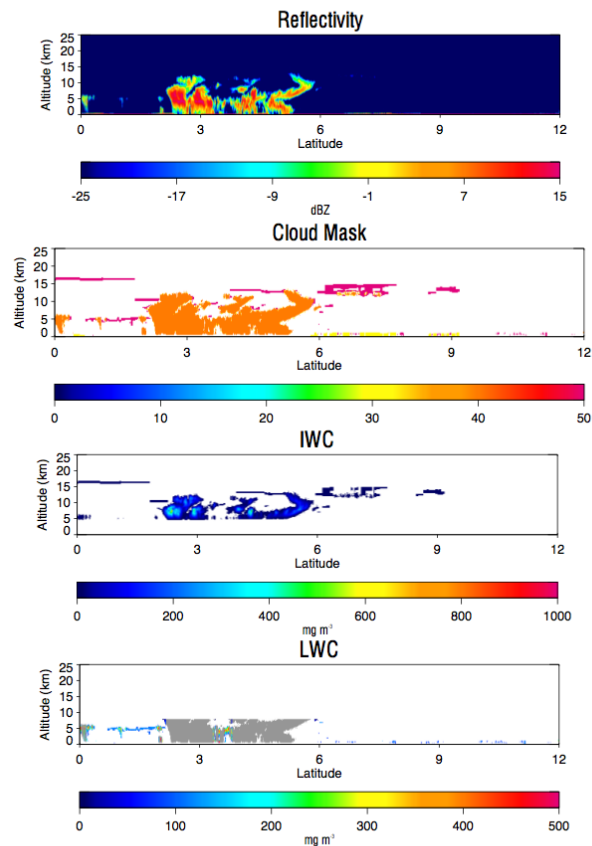

Figure 2: Inputs to 2B-FLXHR-LIDAR from a portion of granule 03616 between 0 and 12°N. Observed reflectivities from 2B-GEOPROF is shown in the upper panel, the cloud mask from 2B-GEOPROF with additional clouds detected by CALIPSO products included in the second panel, while the lower two show retrieved IWC and LWC derived from the 2B-CWC, MOD06-1KM-AUX, and CALIPSO products.

This section of orbit illustrates a number of important aspects of the 2B-FLXHR-LIDAR algorithm. First, note that the gray areas for LWC on Figure 2 correspond to regions for which the 2B-CWC-RO algorithm failed to converge, generally as a result of precipitation in the satellites FOV. As noted in Section 2.2.3, these profiles are modeled by assuming a threshold water content by type of precipitation and is indicated as being cloudy according to the 2B-GEOPROF product. The second panel displays the 2B-FLXHR-LIDAR Cloud/Aerosol mask. Included in the mask are: clouds detected only by CloudSat (Orange), cloud detected only by CALIPSO (Dark Pink), and aerosol detected by CALIPSO (Yellow). It is noted that CALIPSO clouds include full cloud layers as well as cloud top and base undetected by CloudSat. LWC and IWC are filled for these clouds by methods again described in Section 2.2.3.

Qualitative inspection of the scene in Figure 3 illustrates features commonly found in a typical 2B-FLHXR-LIDAR granule. The most interesting of these is the precipitating cloud system between 2 and 8°N that demonstrates a narrow layer of LW cloud top cooling followed by a deeper layer of warming resulting from the deeper penetration of SW radiation into

the cloud. LW warming at cloud base is also evident where precipitation extends to the surface. In the clear-sky regions LW cooling generally dominates the middle atmosphere while a ubiquitous layer of stratospheric heating exists above 15 km. In the lower atmosphere, cloud top cooling can be visualized where new boundary layer clouds are added from CALIOP and SW heating exists where aerosol is located.
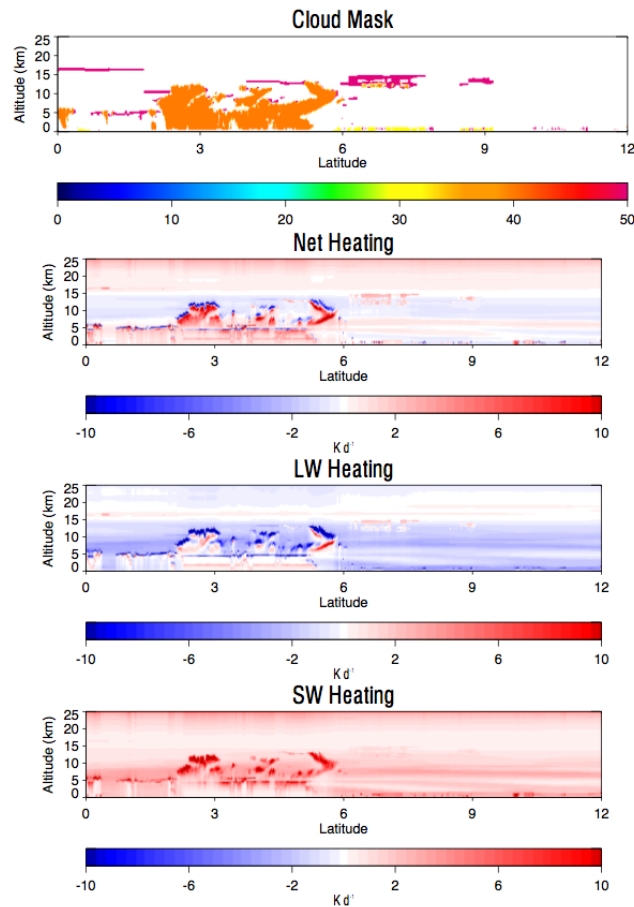

Figure 3: 2B-FLXHR-LIDAR output corresponding to the input shown in Figure 2. The combined cloud and aerosol mask is repeated in the upper panel for reference while the remaining panels show vertical cross-sections of Net, LW and SW radiative heating rates, respectively.

6.2   Cloud Optical Depth example

The R05 2B-FLXHR-LIDAR product now includes vertically resolved cloud optical depth for SW and LW fequencies. An example of the SW optical depth from an orbial segment in granule 16895 is shown in Figure 4. There are multpile interesting features shown here. First, the optical depth in a raining scenario is shown near pixel 13820. Here the transition from rain, to cloud, to liquid water mixed with ice above the freezing level is observed. Detrained ice can be seen and clouds under optical mixed phase regions and thin cirrus are detected; demonstrating the vertically resolved optical depths in multi-layer cloud profiles. Looking at a more expanded region from granule 16890, collocated column optical depths from the MOD06-1KM-AUX product are shown in 5 between the 2B-FLXHR-LIDAR optical depths and those from MODIS.
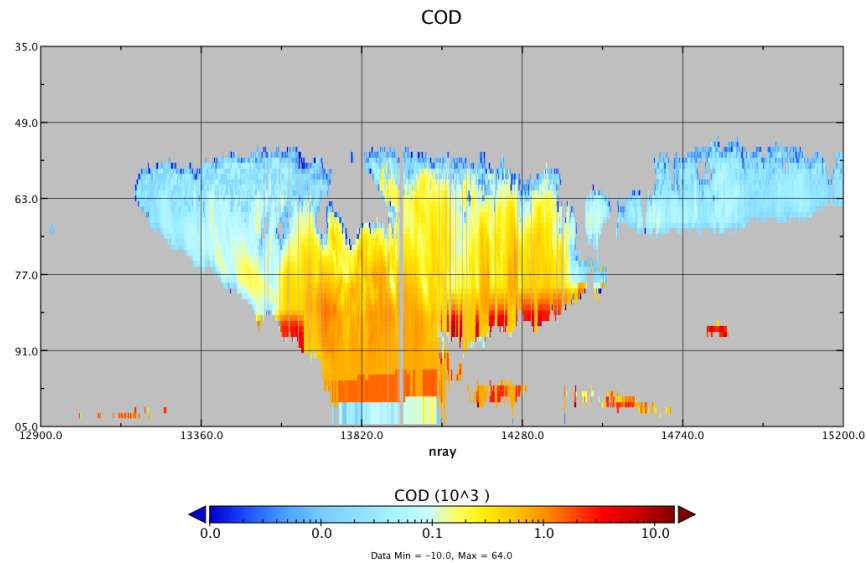
Figure 4: 2B-FLXHR-LIDAR output corresponding a segment of SW cloud optical depth in granule 16895. Created using the Panapoly data visualizer.
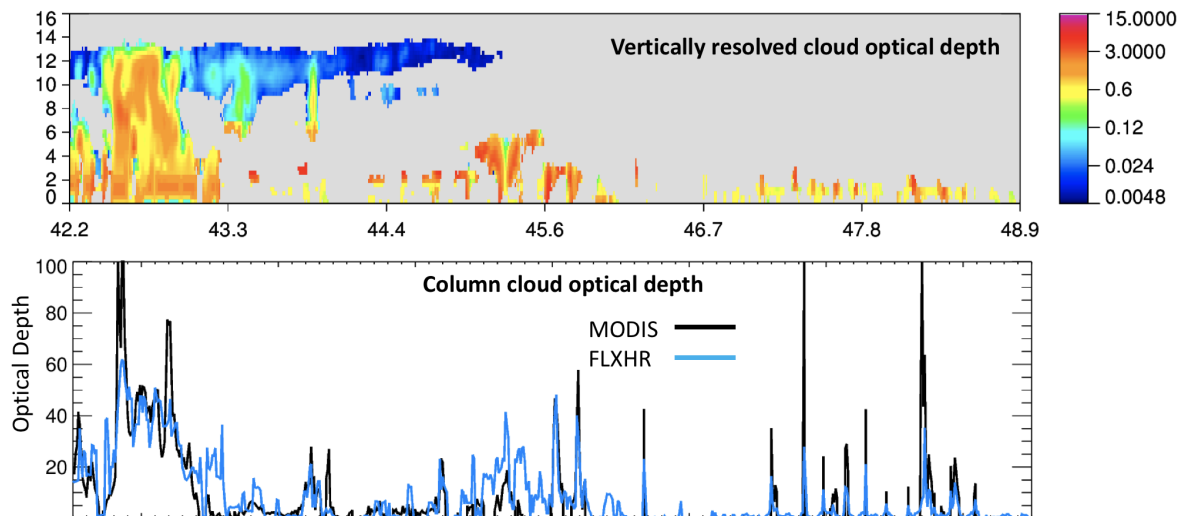

Figure 5: Column optical depths from 2B-FLXHR-LIDAR output and collocated MODIS data (granule 16890).

7   Operator Instructions

The 2B-FLXHR-LIDAR algorithms are implemented in concert with the other level 2 algorithms as a component in the CloudSat Operational and Research Environment (CORE). As the final link in CloudSat's Level 2 product chain, 2B-FLXHR-LIDAR output is not directly used by any other algorithm but depends, either directly or indirectly, on almost all other level 2 products. Thus the 2B-FLXHR-LIDAR algorithm will only be run on pixels for which all other level 2 algorithms were successful. All other pixels will be flagged as missing data by assigning a value of -999 and skipped. Since this type of missing data is entirely based on prior products, it is assumed that any serious flaws in the processing

chain owing to prior algorithms will have already been discovered. As a result no additional quality assessment is proposed regarding this type of missing data.

For all pixels with valid data in all other level 2 products, the quality of the 2B-FLXHR-LIDAR output will be evaluated on a pixel-by-pixel basis for unphysical flux estimates. Since the broadband radiative transfer model employed in the 2B-FLXHR-LIDAR algorithm has been extensively tested and is implemented in numerous other forms, its failure is unlikely and it is anticipated that the algorithm will produce reasonable output provided the appropriate 2B-LWC and 2B-IWC inputs are available. To ensure this is the case a simple threshold test will be employed. If any flux exceeds 1500 Wm^{-2}, all output for that pixel will be flagged as missing by assigning a value of -999. Likewise if any flux goes negative, all output data will be similarly flagged. These thresholds should never be exceeded even under unusual circumstances so, in the event that more than 10 such pixels occur within any orbit, a warning message will be relayed through the on-screen summary to alert the operator of a possible problem with the algorithm.

A second, more comprehensive quality assessment tool will be provided through a statistical summary of the 2B-FLXHR-LIDAR algorithms flux and heating rate estimates that will also be stored in the HDF-EOS output file for each orbit. Statistics regarding the number of breakdown of all CloudSat rays in each orbit into the output categories defined by the status flag (Table 17) will be stored in an additional metadata field called "Flag counts". In addition, mean and standard deviation statistics for fluxes at the atmospheric boundaries (top of the atmosphere and surface) will be computed for each value of the status flag over the latitude bands summarized in Table 19. These variables, stored as additional output data, will ordinarily be used to construct estimates of regional radiation budgets but can also be monitored by the operator to detect systematic variations in the algorithms performace with time and used by algorithm developers to trace the source of any errors that occur. A change of more than 25 % from one orbit to the next in any of the mean longwave flux estimates (MeanOLR, MeanSLR, MeanSFCE, or MeanQLW) is indicative of a potential problem with the algorithm

The final tool for quality assessment of the 2B-FLXHR-LIDAR products consists of a plot of the downwelling longwave flux over the entire orbit. The gross features in this plot should resemble those found in the other L2B products. In particular, the tops of clouds identified in the 2B-CLDCLASS-LIDAR product should be very well defined in the corresponding downwelling longwave flux field.

8 Acronym List

CALIOP Cloud-Aerosol Lidar with Orthogonal Polarization

CALIPSO Cloud-Aerosol Lidar and Infrared Pathfinder Satellite Observation

CIRA Cooperative Institute for Research in the Atmosphere

CERES Clouds and the Earth's Radiant Energy System

CPR Cloud Profiling Radar

EOS Earth Observing System

HDF Hierarchical Data Format

IFOV Instantaneous Field of View

IWC Ice Water Content

LWC Liquid Water Content

MODIS Moderate Resolution Imaging Spectrometer

QC Quality Control

SDS Scientific Data Set

SFC Surface

SPRINTARS Spectral Radiation-Transport Model for Aerosol Species

TOA Top of Atmosphere

VTCW Vehicle Time Code Word

References

[1] Stephens, G. L., P. M. Gabriel and P. T. Partain, 2001: "Parameterization of atmospheric radiative transfer. Part I: validity of simple models," J.Atmos.Sci., 48, 3391 - 3409.

[2] Stephens, G. L. and P. J. Webster, 1981: "Clouds and climate: Sensitivity of simple systems," J. Atmos. Sci., 38, 235-247.

[3] Fu, Q. and K. N. Liou, 1992: "On the correlated k-distribution method for radiative transfer in nonhomogeneous atmospheres," J. Atmos. Sci., 49, 2139 - 2156.

[4] Ritter, B. and J.-F. Geleyn, 1992: "A comprehensive radiation scheme for numerical weather prediction models with potential applications in climate simulations," Mon. Wea. Rev., 120, 303 - 324.

[5] Stephens, G. L., P. W. Stackhouse, Jr., and F. J. Flatau, 1990: "The relevance of the microphysical and radiative properties of cirrus clouds to climate and climate feedback," J. Atmos. Sci., 47, 1742 - 1753.

[6] Mace, G. G., Q. Zhang, M. Vaughan, R. Marchand, G. Stephens, C. Trepte, and D.Winker, 2008: "A description of hydrometeor layer occurrence statistics derived from the first year of merged Cloudsat and CALIPSO data," J. Geophys. Res., 114,D00A26. doi:10.1029/2007JD009755.

[7] Haladay, T. and G. Stephens, 2009: "Characteristics of tropical thin cirrus clouds deduced from joint CloudSat-CALIPSO observations," J. Geophys. Res., 114:D00A25. doi:10.1029/2008JD010675

[8] LEcuyer, T., N. Wood, T. Haladay, G. L. Stephens, and P. W. Stackhouse, 2008: "Impact of clouds on atmospheric heating based on the R04 CloudSat fluxes and heating rates dataset." J. Geophys. Res., 113:D00A15. doi:10.1029/2008JD009951..

[9] DAlmeida, G. A., P. Koepke, and E. P. Shettle, 1991: Atmospheric Aerosols: Global Climatology and Radiative Characteristics. A. Deepak, 561 pp.

[10] Takemura, T., T. Nakajima, O. Dubovik, B. N. Holben, and S. Kinne, 2002: Single-scattering albedo and radiative forcing of various aerosol species with a global three-dimensional model. J. Climate, 15:333ï¿½352.

[11] WCP-55, 1983: Report of the expert meeting on aerosols and their climate effects. World Meteorological Organization, Geneva, 107 pp.

[12] Mitchell, D. L., A. Macke, and Y. Liu, 1996: "Modeling cirrus clouds. Part II: Treatment of radiative properties," J. Atmos. Sci., 53, 2967 - 2988.

[13] Clough, S. A., F. X. Kneizys, and R. W. Davies, 1989: "Line shape and the water vapor continuum," Atmos. Res., 23, 229 - 241.

[14] Lacis, A. A., and V. Oinas, 1991: "A description of the correlated k distribution method for modeling nongray gaseous absorption, thermal emission, and multiple scattering in vertically inhomogeneous atmospheres," J. Geophys. Res., 96, 9027 - 9063.

[15] Mace, G., R. Marchand, and Q. Zhang, 2004: Level 2B GEOPROF Process Description and Interface Control Document, NASA Jet Propulsion Laboratory, Pasadena, CA, 43 pp.

[16] Henderson, D. S., T. LEcuyer, G. Stephens, P. Partain, and M. Sekiguchi, 2013: A multisensor perspective on the radiative impacts of clouds and aerosols. J. Appl. Meteor. Climatol., 52, 853-871

[17] Matus, A. V., T. S. LEcuyer, and D. S. Henderson, 2019: New estimates of aerosol direct radiative effects and forcing from A-Train satellite observations. Geophys. Res. Letters

[18] Matus, A. and T. LEcuyer, 2017: The role of cloud phase in Earth's radiation budget. J. Geophys. Res. Atmos., 122, 2559-2578

[19] McIlhattan, E. A., T. S. LEcuyer, and N. B. Miller, 2017: Observational Evidence Linking Arctic Supercooled Liquid Cloud Biases in CESM to Snowfall Processes. Journal of Climate, 30, 4477-4495

[20] Van Tricht, K., S. Lhermitte, J. T. M Lenaerts, I. V. Gorodetskaya, T. LEcuyer, B. Noel, M. R. van den Broeke, D. D. Turner, and N. P. M. van Lipzig, 2016: Clouds enhance Greenland ice sheet meltwater runoff. Nature Communications, 7,

[21] Huang, X. L., X. H. Chen, D. Zhou, and X. Liu, 2016: An observationally based global band-by-band surface emissivity dataset for climate and weather simulations. J. Atmos. Sci., 73

[22] Wang, Z. and K. Sassen, 2001: Cloud type and macrophysical property retrieval using multiple remote sensors. J. Appl. Meteor., 40, 1665-1682.

[23] Pistone, K., Redemann, J., Doherty, S., Zuidema, P., Burton, S., Cairns, B., Cochrane, S., Ferrare, R., Flynn, C., Freitag, S., Howell, S. G., Kacenelenbogen, M., LeBlanc, S., Liu, X., Schmidt, K. S., Sedlacek III, A. J., Segal-Rozenhaimer, M., Shinozuka, Y., Stamnes, S., van Diedenhoven, B., Van Harten, G., and Xu, F., 2019: Intercomparison of biomass burning aerosol optical properties from in situ and remote-sensing instruments in ORACLES-2016, Atmos. Chem. Phys., 19, 9181-9208